SIBE2017 The Third International Conference on Sustainable Infrastructure and Built Environment

On the Accuracy and Convergence of the Hybrid FE-meshfree Q4-CNS Element in Surface Fitting Problems

Foek Tjong Wong[1], Richo Michael Soetanto[2] & Januar Budiman[3]

Master Program of Civil Engineering, Petra Christian University, Surabaya, Indonesia
Email: [1] wftjong@petra.ac.id, [2] hore_yippie@yahoo.co.id, [3] januar@petra.ac.id

Abstract. In the last decade, several hybrid methods combining the finite element and meshfree methods have been proposed for solving elasticity problems. Among these methods, a novel quadrilateral four-node element with continuous nodal stress (Q4-CNS) is of our interest. In this method, the shape functions are constructed using the combination of the 'non-conforming' shape functions for the Kirchhoff's plate rectangular element and the shape functions obtained using an orthonormalized and constrained least-squares method. The key advantage of the Q4-CNS element is that it provides the continuity of the gradients at the element nodes so that the global gradient fields are smooth and highly accurate. This paper presents a numerical study on the accuracy and convergence of the Q4-CNS interpolation and its gradients in surface fitting problems. Several functions of two variables were employed to examine the accuracy and convergence. Furthermore, the consistency property of the Q4-CNS interpolation was also examined. The results show that the Q4-CNS interpolation possess a bi-linier order of consistency even in a distorted mesh. The Q4-CNS gives highly accurate surface fittings and possess excellent convergence characteristics. The accuracy and convergence rates are better than those of the standard Q4 element.

Keywords: *continuous nodal stress; finite element; meshfree; Q4-CNS; quadrilateral four-node element; surface fitting.*

1 Introduction

The finite element method (FEM) is now a widely-used, well-establish numerical method for solving mathematical models of practical problems in engineering and science. In practice, FEM users often prefer to use simple, low order triangular or quadrilateral elements in 2D problems and tetrahedral elements in 3D problems since these elements can be

Received ________, Revised _________, Accepted for publication __________

automatically generated with ease for meshing complicated geometries. Nevertheless, the standard low order elements produce discontinuous gradient fields on the element boundaries and their accuracy is sensitive to the quality of the mesh.

To overcome the FEM shortcomings, since the early 1990's up to present a vast amount of meshfree (or meshless) methods [1], [2], which do not require a mesh in discretizing the problem domain, have been proposed. A recent review on meshfree methods presented by Liu [3]. While these newer methods are able to eliminate the FEM shortcomings, they also have their own, such as: (i) the computational cost is much more expensive than the FEM, and (ii) the computer implementation is quite different from that of the standard FEM.

To synergize the strengths of the finite element and meshfree methods while avoiding their weaknesses, in the last decade several hybrid methods combining the two classes of methods based on the concept of partition-of-unity have been developed [4]-[8]. Among several hybrid methods available in literature, the authors are interested in the four-node quadrilateral element with continuous nodal stress (Q4-CNS) proposed by Tang el al. [6] for the reason that this work is the pioneering hybrid method possessing the property of continuous nodal stress. The Q4-CNS can be regarded as an improved version of the FE-LSPIM Q4 [4], [5]. In this novel method, the nonconforming shape functions for the Kirchhoff's plate rectangular element are combined with the shape functions obtained using an orthonormalized and constrained least-squares method. The advantages of the Q4-CNS are [6], [9], [10]: (1) the shape functions are C^1 continuous at nodes so that it naturally provides a globally smooth gradient fields. (2) The Q4-CNS can give higher accuracy and faster convergence rate than the standard quadrilateral element (Q4). (3) The Q4-CNS is more tolerant to mesh distortion.

The Q4-CNS has been developed and applied for the free and forced vibration analyses of 2D solids [9] and for 2D crack propagation analysis [10]. Recently the Q4-CNS has been further developed to its 3D counterpart, that is, the hybrid FE-meshfree eight-node hexahedral element with continuous nodal stress (Hexa8-CNS) [11]. However, examination of the Q4-CNS interpolation in fitting surfaces defined by functions of two variables has not been carried out. Thus, it is the purpose of this paper to present a numerical study on the on the accuracy and convergence of the Q4-CNS shape functions and their derivatives in surface fitting problems. Furthermore, the consistency (or completeness) property of the Q4-CNS shape functions is numerically examined in this study.

2 The Q4-CNS Interpolation

As in the standard finite element procedure, a 2D problem domain, $\bar{\Omega}$, is firstly divided into four-node quadrilateral elements to construct the Q4-CNS shape functions. Consider a typical element $\bar{\Omega}^e$ with the local node labels 1, 2, 3 and 4. The unknown function *u* on the interior and boundary of the element is approximated by

$$u^h(x,y) = \sum_{i=1}^{4} w_i(\xi,\eta) u_i(x,y) \tag{1}$$

where $w_i(\xi,\eta)$ and $u_i(x,y)$ are the weight functions and nodal approximations, respectively, associated with node *i*, *i*=1,…,4. Note that in the classical isoparametric four-node quadrilateral element (Q4), the weight functions are given as the shape functions and the nodal approximations are reduced to nodal values u_i. The weight functions in the Q4-CNS are defined as the non-conforming shape functions for the Kirchhoff's plate rectangular element [6], [12], that is,

$$w_i(\xi,\eta) = \tfrac{1}{8}(1+\xi_0)(1+\eta_0)(2+\xi_0+\eta_0-\xi^2-\eta^2), \tag{2a}$$

$$\xi_0 = \xi_i \xi, \quad \eta_0 = \eta_i \eta, \quad i=1,2,3,4. \tag{2b}$$

where ξ and η are the natural coordinates of the classical Q4 with the values in the range of –1 to 1. The weight functions satisfy the partition of unity property, that is, $\sum_1^4 w_i(\xi,\eta)=1$. The nodal approximations $u_i(x,y)$ are constructed using the orthonormalized and constrained least-squares method (CO-LS) as presented by Tang et al. [6] and Yang et al. [9], [10]. Here the CO-LS is briefly reviewed.

To construct the CO-LS approximation, nodal support domains of node i, $\bar{\Omega}_i$, i=1,…,4 of a typical quadrilateral element $\bar{\Omega}^e$ are firstly defined using the neighboring nodes of node i. For example, the nodal support domain of node 3 of element e is shown in Fig. 1(a). The element support domain $\hat{\Omega}^e$ is then defined as the union of the four nodal support domains, that is, $\hat{\Omega}^e = \cup_1^4 \bar{\Omega}_i$, as shown in Fig. 1(b).

Consider a nodal support domain of node i, $\bar{\Omega}_i$ with the total number of supporting nodes n. Let the labels for the nodes be j, j=1,…, n. Using the least-squares method, the nodal approximation $u_i(x,y)$ is given as

$$u_i(x,y) = \mathbf{p}^{\mathrm{T}}(x,y)\mathbf{A}^{-1}\mathbf{B}\mathbf{a} \tag{3}$$

where $\mathbf{p}(x, y)$ is a vector of polynomial basis functions, viz.

$$\mathbf{p}^{\mathrm{T}}(x,y) = \{1 \quad x \quad y \quad x^2 \quad xy \quad y^2 \quad \cdots \quad \} \quad (1\times m) \tag{4}$$

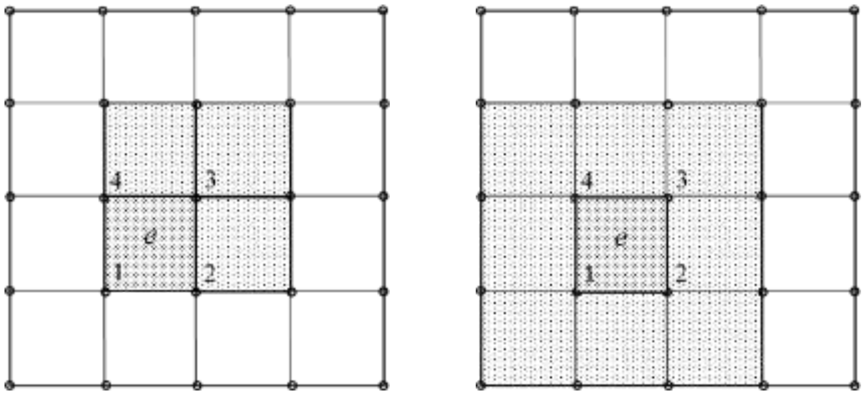

(a) $\bar{\Omega}_3$ (b) $\hat{\Omega}^e$

Figure 1 Definitions of: (a) the nodal support domain of node 3 of element *e* and (b) the element support domain of element *e*.

Here m is the number of monomial bases in $\mathbf{p}$. Following the original work [6], in this study the 'serendipity' basis function $\mathbf{p}^{\mathrm{T}}(x,y)=\{1 \quad x \quad y \quad x^2 \quad xy \quad y^2 \quad x^2y \quad xy^2\}$ is used if $n>8$ and the bi-linear basis function $\mathbf{p}^{\mathrm{T}}(x,y)=\{1 \quad x \quad y \quad xy\}$ is used if $n\le 8$. Matrices $\mathbf{A}$ and $\mathbf{B}$ are the moment matrix and the basis matrix, respectively, given as

$$\mathbf{A}=\sum\nolimits_{j=1}^{n}\mathbf{p}(x_j,y_j)\mathbf{p}^{\mathrm{T}}(x_j,y_j) \qquad (m\times m) \tag{5}$$

$$\mathbf{B}=\left[\mathbf{p}(x_1,y_1) \quad \mathbf{p}(x_2,y_2) \quad \cdots \quad \mathbf{p}(x_n,y_n)\right] \qquad (m\times n) \tag{6}$$

Vector $\mathbf{a}=\{a_1 \quad a_2 \quad \cdots \quad a_n\}^{\mathrm{T}}$ is the vector of nodal parameters. Note that in general vector $\mathbf{a}$ is *not* a vector of nodal values because the approximation $u_i(x,y)$ does not necessarily pass through the nodal values.

Defining the inner product for any two basis functions $f(x,y)$ and $g(x,y)$ as

$$\left(f(x,y),g(x,y)\right)=\sum_{j=1}^{n} f(x_j,y_j)g(x_j,y_j) \quad (7)$$

and using the Gram-Schmidt orthonormalization algorithm [6], the basis vector **p** can be transformed into an orthonormal basis function vector **r** so that the moment matrix **A** becomes the identity matrix. Subsequently, the nodal approximation is constrained using the Lagrange multiplier method so that the nodal parameter $u_i(x,y)$ at node i is equal to the nodal value u_i. Going through the abovementioned process, the nodal approximation, Eqn. (3), turns into

$$u_i(x,y)=\mathbf{\Phi}(x,y)\mathbf{a}=\sum_{j=1}^{n}\phi_j^i(x,y)a_j \quad (8)$$

where

$$\mathbf{\Phi}(x,y)=\begin{bmatrix}\phi_1^i(x,y) & \phi_2^i(x,y) & \cdots & \phi_n^i(x,y)\end{bmatrix}=\mathbf{r}^{\mathrm{T}}(x,y)\mathbf{B}^i \quad (9)$$

$$\mathbf{B}^i=\begin{bmatrix}\mathbf{B}_1^i & \mathbf{B}_2^i & \cdots & \mathbf{B}_n^i\end{bmatrix} \quad (10)$$

$$\mathbf{B}_j^i=\mathbf{r}(x_j,y_j)-f_j^i\mathbf{r}(x_i,y_i)\,,\quad j=1,\ldots,n \quad (11)$$

$$f_j^i=\begin{cases}(\mathbf{r}^{\mathrm{T}}(x_i,y_i)\mathbf{r}(x_j,y_j))\big/(\mathbf{r}^{\mathrm{T}}(x_i,y_i)\mathbf{r}(x_i,y_i)) & \text{if } j\neq i\\ (\mathbf{r}^{\mathrm{T}}(x_i,y_i)\mathbf{r}(x_j,y_j)-1)\big/(\mathbf{r}^{\mathrm{T}}(x_i,y_i)\mathbf{r}(x_i,y_i)) & \text{if } j=i\end{cases} \quad (12)$$

Note that n, the number of nodes in the nodal support domain of node i, in general varies with i.

Consider now the element support domain of element *e*, $\hat{\Omega}^e$, with the total number of nodes *N*. Let the node labels in $\hat{\Omega}^e$ be *I*=1, …, *N*. Using this element level labelling system and substituting Eqn. (8) into Eqn. (1), the approximate function can be expressed as

$$u^h(x,y) = \sum_{i=1}^{4} w_i(\xi,\eta) \sum_{I=1}^{N} \phi_I^i(x,y) a_I = \sum_{I=1}^{N} \psi_I(x,y) a_I \tag{13}$$

in which $\psi_I(x,y)$ is the Q4-CNS shape function associated with node *I* in the element support domain. In this equation, if node *I* is not in the nodal support domain of node *i*, then $\phi_I^i(x,y)$ is defined to be zero. It is obvious that the shape function is the product of the nonconforming rectangular element shape functions $w_i(\xi,\eta)$ and the CO-LS shape functions $\phi_I^i(x,y)$, that is,

$$\psi_I(x,y) = \sum_{i=1}^{4} w_i(\xi,\eta) \phi_I^i(x,y) \tag{14}$$

3 Numerical Tests

In this section, the accuracy and convergence of the Q4-CNS interpolation in fitting surfaces of $z = f(x,y)$ and their derivatives are examined. To measure the approximation errors, the following relative L_2 norm of error is used

$$r_z = \sqrt{\frac{\int_{\Omega^h} (z - z^h)^2 \, dA}{\int_{\Omega^h} z^2 \, dA}} \tag{15}$$

in which z is the function under consideration, z^h is the approximate function, and Ω^h is the approximate domain with the element characteristic size, h. This expression is also applicable to measure the relative error of the function partial derivatives (replacing z and z^h with their derivatives). The integral in Eqn. (15) is evaluated numerically using Gaussian quadrature rule. The number of quadrature sampling points is taken to be 5×5. For the purpose of comparison, the accuracy and convergence of the standard Q4 interpolation and its partial derivatives are also presented.

3.1 Shape function consistency property

In order to be applicable as the basis functions in the Rayleigh-Ritz based numerical method, a set of shape functions is required to be able to represent exactly all polynomial terms of order up to m in the Cartesian coordinates [13], where m is the variational index (that is, the highest order of the spatial derivatives that appears in the problem functional). A set of shape functions that satisfies this condition is called m-consistent [13]. This consistency property is a *necessary* condition for convergence (that is, as the mesh is refined, the solution approaches to the exact solution of the corresponding mathematical model).

To examine the consistency property of the Q4-CNS shape functions, consider a 10×10 square domain shown in Fig. 2. The domain is subdivided using 4×4 regular quadrilateral elements, Fig. 2(a), and irregular quadrilateral elements, Fig. 2(b). The functions under consideration are the polynomial bases up to the quadratic bases, that is, $z=1$, $z=x$, $z=y$, $z=xy$, $z=x^2$ and $z=y^2$. The results of the relative errors for the Q4-CNS interpolation and its nonzero partial derivatives are listed in Tables 1 and 2, respectively, together with those of the standard Q4 interpolation.

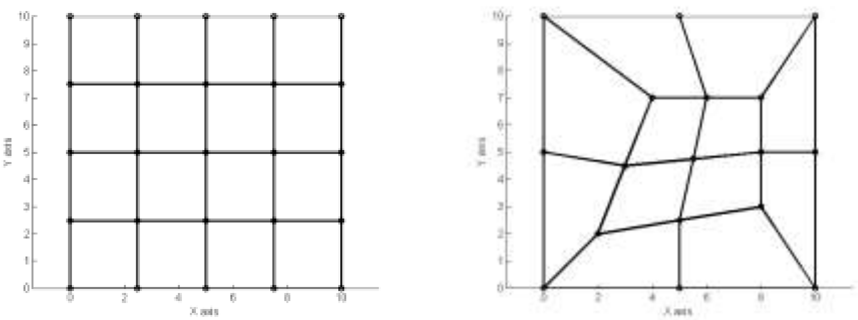

(a) Regular mesh (b) Irregular mesh

Figure 2 Square function domain of size 10-by-10 subdivided into: (a) regular and (b) irregular quadrilateral elements.

Table 1 Relative L_2 norm of errors for the approximation of different polynomial basis functions using the regular and irregular meshes.

Function	**Regular Mesh**		**Irregular Mesh**	
	Q4-CNS	**Q4**	**Q4-CNS**	**Q4**
$z=1$	9.98E-16	1.32E-17	1.88E-15	1.35E-17
$z=x$	1.41E-15	0	2.82E-15	0
$z=y$	1.20E-15	0	1.45E-15	0
$z=xy$	1.39E-15	1.49E-16	4.59E-15	2.37%
$z=x^2$	1.22%	2.55%	2.65%	5.83%
$z=y^2$	1.22%	2.55%	2.33%	5.37%

Table 2 Relative L_2 norm of errors for the approximation of nonzero polynomial basis function derivatives using the regular and irregular meshes.

(a) Basis function derivatives with respect to x

Function Derivative to x	**Regular Mesh**		**Irregular Mesh**	
	Q4-CNS	**Q4**	**Q4-CNS**	**Q4**
$Z_{,x}=1$	9.11E-15	2.25E-16	2.15E-14	2.82E-16
$Z_{,x}=y$	9.36E-15	2.55E-16	3.06E-14	11.32%
$Z_{,x}=2x$	6.70%	12.50%	10.94%	16.58%

(b) Basis function derivatives with respect to y

Function Derivative to y	**Regular Mesh**		**Irregular Mesh**	
	Q4-CNS	**Q4**	**Q4-CNS**	**Q4**
$Z_{,y}=1$	8.71E-15	1.98E-16	9.61E-15	2.11E-16
$Z_{,y}=x$	1.02E-14	2.93E-16	3.58E-14	12.53%
$Z_{,y}=2y$	6.70%	12.50%	10.30%	15.90%

The tables show that the Q4-CNS interpolation is capable to reproduce exact solutions up to the *xy* basis both for the domain with regular and irregular meshes. In other words, the Q4-CNS interpolation is consistent up to the *xy* basis. On the other hand, the Q4 interpolation is consistent up to the same basis for the regular mesh, but it is only purely linear consistent for the irregular mesh. This finding may partly explain the reason the Q4-CNS has higher tolerance to mesh distortion [6]. For the x^2 and y^2 bases, both the Q4-CNS and Q4 interpolations are not able to produce the exact solutions, as expected. For these bases, the Q4-CNS interpolation is consistently more accurate than the standard Q4.

The tables clearly reveals that the Q4-CNS interpolation is not consistent up to all of the quadratic bases. As a consequence, the Q4-CNS is not applicable to variational problems possessing variational index m=2, including the Love-Kirchhoff plate bending and shell models. This is in contradiction to the statement made in the original paper [6], which mentioned that the Q4-CNS "is potentially useful for the problems of bending plate and shell models". If the Reissner-Mindlin theory is adopted, however, the Q4-CNS is of course applicable.

3.2 Accuracy and Convergence

3.2.1 Quadratic function

The accuracy and convergence of the Q4-CNS interpolation in fitting functions in 2D domain are firstly examined using quadratic function (adapted from an example in Wong and Kanok-nukulchai [14]) given as

$$z = 1 - x^2 - y^2 \tag{16}$$

with two different domains, viz.

$$\overline{\Omega}_S = \{(x, y) | 0 \le x \le 1, \ 0 \le y \le 1\} \tag{17}$$

$$\overline{\Omega}_C = \{(x, y) | x^2 + y^2 \le 1, x \ge 0, y \ge 0\} \tag{18}$$

The first domain, Eqn. (17), is the unit square while the second one, Eqn. (18), is a quarter of the unit circle, both of which are located in the first quadrant of the Cartesian coordinate system. The unit square is subdivided using regular meshes of 2×2, 4×4, 8×8, and 16×16 square elements. The quarter of the unit circle is subdivided into 3, 12, 27, and 48 quadrilateral elements as shown in Fig. 3 (taken from an example in Katili [15]).

The relative error norms of the Q4-CNS and Q4 interpolations in approximating the quadratic function, Eqn. (16), and its partial derivatives, are presented in Table 3 for the square domain and in Table 4 for the quarter circle domain. The tables show that the Q4-CNS interpolation converges very well to the quadratic function *z* both for the regular mesh in the unit square domain and for the relatively irregular mesh in the quarter of the unit circle domain. The tables also confirm that the Q4-CNS interpolation is consistently more accurate than the Q4 interpolation. The finer the mesh the more accurate the Q4-CNS interpolation compared to the Q4.

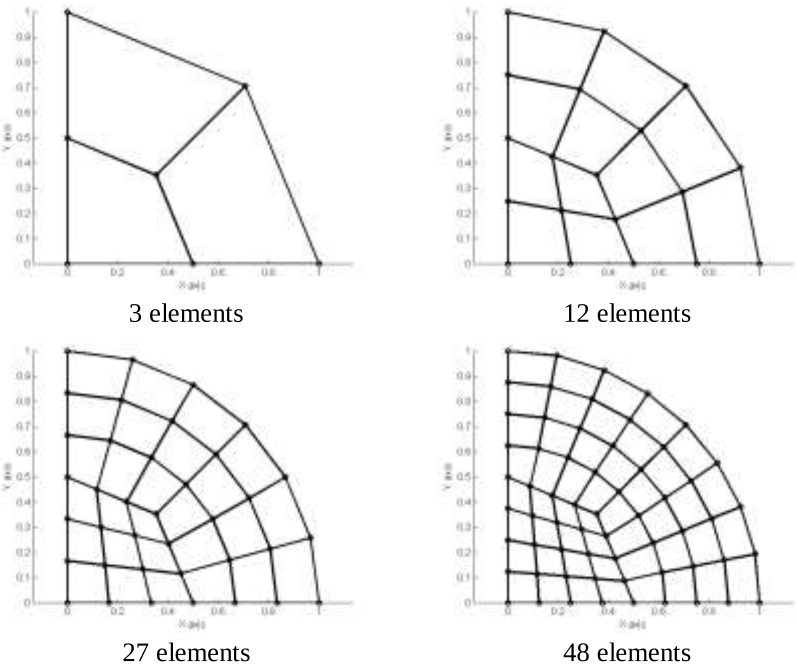

Figure 3 A quarter of the unit circle subdivided into different number of quadrilateral elements (Katili [15], p.1899).

Table 3 Relative L_2 norm of errors for the approximation of the quadratic function, r_z, and its partial derivatives, $\boldsymbol{r_{z,x}}$ and $\boldsymbol{r_{z,y}}$ over the unit square domain.

M	$\boldsymbol{r_z}$		$\boldsymbol{r_{z,x}}$		$\boldsymbol{r_{z,y}}$	
	Q4-CNS	**Q4**	**Q4-CNS**	**Q4**	**Q4-CNS**	**Q4**
2	10.18%	16.26%	22.77%	25.00%	26.29%	28.87%
4	1.83%	4.07%	10.62%	12.50%	12.26%	14.43%
8	0.33%	1.02%	4.13%	6.25%	4.77%	7.22%
16	0.06%	0.25%	1.52%	3.13%	1.76%	3.61%

M: the number of elements on each edge

Table 4 Relative L_2 norm of errors for the approximation of the quadratic function, r_z, and its partial derivatives, $\boldsymbol{r_{z,x}}$ and $\boldsymbol{r_{z,y}}$ over a quarter of the unit circle domain.

Number of elements	r_z		$r_{z,x}$		$r_{z,y}$	
	Q4-CNS	Q4	Q4-CNS	Q4	Q4-CNS	Q4
3	11.06%	16.59%	28.14%	33.92%	22.48%	27.10%
12	2.51%	4.52%	14.56%	16.16%	12.57%	13.96%
27	0.91%	2.04%	8.42%	10.68%	7.37%	9.36%
48	0.44%	1.15%	5.64%	7.99%	4.97%	7.03%

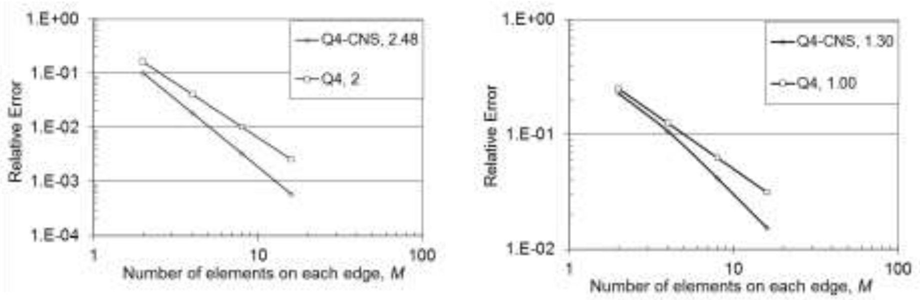

(a) Relative error norms of interpolations

(b) Relative error norms of interpolation x-partial derivative

Figure 4 Convergence of the Q4-CNS and Q4 interpolations in approximating: (a) the quadratic function, (b) the partial derivatives of the function with respect to x, over the unit square. The number in the legend indicate the average convergence rate.

The relative error norms are plotted against the number of elements on each edge, M, in log-log scale as shown in Fig. 4. The convergence graphs for the partial derivatives with respect to y are similar to Fig. 4(b) and have the same convergence rates. The graphs show that the average convergence rate of the Q4-CNS interpolation is about 25% faster than that of the Q4. It is worth mentioning here that the convergence rates of the Q4 interpolation, 2, and its partial derivatives, 1, are exactly the same as predicted by the interpolation theory [16].

3.2.2 Cosine function

The second function chosen to examine the accuracy and convergence of the Q4-CNS interpolation is

$$z = \cos(\frac{\pi}{2}x)\cos(\frac{\pi}{2}y) \tag{19}$$

defined over the square unit domain, Eqn. (17). The meshes used are the same as those in the previous example.

The convergence graphs of the relative error norms of the Q4-CNS and Q4 interpolations and their partial derivatives with respect to *x* are shown in Fig. 5. The graphs confirm the superiority of the Q4-CNS interpolation over the Q4 interpolation both in terms of the accuracy and convergence rate.

4 Conclusions

The consistency property, accuracy and convergence of the Q4-CNS interpolation in surface fitting problems have been numerically studied. The results show that the Q4-CNS interpolation is consistent up to the bilinear basis both for the regular and irregular meshes. It is more accurate than the Q4 in fitting the functions and their derivatives. In a sufficiently fine mesh, the error norm of the Q4-CNS interpolation is around 3 to 4 times smaller than that of the Q4, and the error norm of its derivatives is around 1.5 to 2 times smaller than that of the Q4. The Q4-CNS interpolation converge very well to the fitted function. Its convergence rate is approximately 25% faster than that of the Q4. The demerits of the present method is that the computational cost to construct the shape function is much higher than the Q4 shape function.

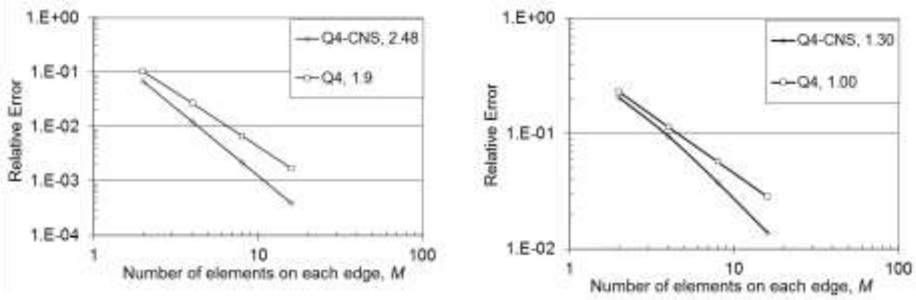

(a) Relative error norms of interpolations

(b) Relative error norms of interpolation of the *x*-partial derivative

Figure 5 Convergence of the Q4-CNS and Q4 interpolations in approximating: (a) the bi-cosine function, (b) the partial derivatives of the function with respect to *x*, over the unit square. The number in the legend indicate the average convergence rate.

Acknowledgement

We gratefully acknowledge that this research is partially supported by the research grant of the Institute of Research and Community Service, Petra Christian University, Surabaya.

5 References

[1] Liu, G.R., *Mesh Free Methods: Moving Beyond the Finite Element Method*, 1st ed., Boca Raton: CRC Press, 1-5, 2003.

[2] Gu, Y.T., *Meshfree Methods and Their Comparisons*, International Journal of Computational Methods, **2**(4), pp. 477–515, 2005.

[3] Liu, G.R., *An Overview on Meshfree Methods: For Computational Solid Mechanics*, International Journal of Computational Methods, **13**(5), pp. 1630001-1–1630001-42, 2016.

[4] Rajendran, S. & Zhang, B.R., *A 'FE-meshfree' Q4 Element Based on Partition of Unity*, Computer Methods in Applied Mechanics and Engineering, **197**(1–4), pp. 128–147, 2007.

[5] Zhang, B.R. & Rajendran, S., '*FE-meshfree' Q4 Element for Free-vibration Analysis*, Computer Methods in Applied Mechanics and Engineering, **197**(45–48), pp. 3595–3604, 2008.

[6] Tang, X.H., Zheng, C., Wu, S.C., & Zhang, J.H., *A Novel Four-node Quadrilateral Element with Continuous Nodal Stress*, Applied Mathematics and Mechanics, **30**(12), pp. 1519–1532, 2009.

[7] Yang, Y., Tang, X.H., & Zheng, H., *A Three-node Triangular Element with Continuous Nodal Stress*, Computers & Structures, **141**, pp. 46–58, 2014.

[8] Yang, Y., Bi, R., & Zheng, H., *A Hybrid 'FE-meshless' Q4 with Continuous Nodal Stress using Radial-polynomial Basis Functions*, Engineering Analysis with Boundary Elements, **53**, pp. 73–85, 2015.

[9] Yang, Y., Chen, L., Xu, D., & Zheng, H., *Free and Forced Vibration Analyses using the Four-node Quadrilateral Element with Continuous Nodal Stress*, Engineering Analysis with Boundary Elements, **70**, pp. 1–11, 2016.

[10] Yang, Y., Sun, G., Zheng, H., & Fu, X., *A Four-node Quadrilateral Element Fitted to Numerical Manifold Method with Continuous Nodal Stress for Crack Analysis*, Computers & Structures, **177**, pp. 69–82, 2016.

[11] Yang, Y., Chen, L., Tang, X.H., Zheng, H., & Liu, Q.S., *A Partition-of-unity Based 'FE-meshfree' Hexahedral Element with*

Continuous Nodal Stress, Computers & Structures, **178**, pp. 17–28, 2017.

[12] Zienkiewicz, O.C. & Taylor, R.L., *The Finite Element Method, Volume 2: Solid Mechanics*, 5th ed., Butterworth-Heinemann, 126, 2000.

[13] Felippa, C.A., *Introduction To Finite Element Methods (ASEN 5007), Fall 2016* , University of Colorado at Boulder, http://www.colorado.edu/engineering/cas/courses.d/IFEM.d/, (14-Oct-2016).

[14] Wong, F. T. & Kanok-Nukulchai, W., *Kriging-based Finite Element Method : Element-by-Element Kriging Interpolation*, Civil Engineering Dimension, **11**(1), pp. 15–22, 2009.

[15] Katili, I., *A New Discrete Kirchhoff-Mindlin Element based on Mindlin-Reissner Plate Theory and Assumed Shear Strain Fields-Part II: an Extended DKQ Element for Thick-Plate Bending Analysis*, International Journal for Numerical Methods in Engineering, **36**(11), pp. 1885–1908, 1993.

[16] Bathe, K.J., *Finite Element Procedures*, Prentice-Hall, 244-250, 1996.